Comparison of choline blood brain barrier and neuronal transport and anticholinesterase inhibitory properties of potential cationic Alzheimers disease drugs

Clifford W Fong

Comparison of choline blood brain barrier and neuronal transport and anticholinesterase inhibitory properties of potential cationic Alzheimers disease drugs

Clifford W. Fong
Eigenenergy, Adelaide, South Australia, Australia.
Email: cwfong@internode.on.net

Keywords: Choline and cationic analogs transporters; Blood brain barrier; neurons; acetylcholinesterase inhibitors; Alzheimer's disease**;** HOMO LUMO quantum mechanics;

Abbreviations

BBB Blood Brain Barrier, Acetylcholine ACh, Acetylcholinesterase AChE, Acetylcholinesterase inhibitors AChEIs**,** AD Alzheimer's disease, Choline transporter ChT, Choline transporter-like protein 1 CTL1, Choline transporter-like protein 2, CTL2 , Organic cation transporter OCT, Structure activity relationships SAR, $\Delta G_{desolv,CDS}$ free energy of water desolvation**,** $\Delta G_{lipo,CDS}$ lipophilicity free energy, CDS cavity dispersion solvent structure of the first solvation shell, Dipole moment DM, Molecular Volume Vol, HOMO highest occupied molecular orbital, LUMO lowest unoccupied molecular orbital, HOMO-LUMO energy gap.

Abstract

It has been shown that there are similarities between the transport of potential choline-like cationic Alzheimer's disease drugs across the blood brain barrier and into neurons compared to the inhibitory binding of acetylcholinesterase. An analysis of water desolvation, lipophilicity, dipole moment, molecular volume, HOMO, LUMO or HOMO-LUMO molecular properties and their impact on transport or inhibitory binding has shown that while lipophilicity, dipole moment, desolvation, and molecular volume are important but varying determinants for transport and inhibitory binding, the HOMO is the important determinant for transport processes, but the LUMO is the more important determinant for the inhibitory binding to acetylcholinesterase. This difference appears to be a general consequence of the higher **π**-cation interaction in the binding gorge of acetylcholinesterase compared to the weaker **π**-cation and hydrophobic interaction of substrates in the pore of the CTL or ChT transporters. Inhibition of AChE is a binding process facilitated by electron transfer from the HOMO of the AChE to the LUMO of the cationic inhibitors, whereas the transportation of cationic species by the CTL and ChT transporters does not involve such a strong binding process, but more a weaker interaction involving electron transfer from the HOMO of the substrates to the LUMO of the transporters that ultimately allows the passage of substrates through the CTL and ChT pores. There is supporting but not explicit evidence in the literature that points to the similarities between the transport of drugs through the blood brain barrier or into neurons when compared to the binding of cationic drugs to acetylcholinesterase.

An analysis of the molecular volumes of the TAK-147 analogs on binding to AChE where the increasing length of the analogs by adding methylene spacing groups leads to an optimum binding interaction with AChE which then decreases with the addition of further spacers is explained by the binding interaction being dependent on the molecular volume and the LUMO.

Introduction

The pathogenesis of Alzheimer's disease (AD) has long been linked to a deficiency in the brain neurotransmitter acetylcholine (ACh), although it is uncertain whether an acetylcholine deficit is the primary pathological cause for AD or rather a consequence of the disease. Acetylcholine esterases (AChE) are responsible for the breakdown of the acetylcholine (ACh) in the normal brain since an excess of ACh would lead to repeated and uncontrolled muscle stimulation. However in an AD patient, inhibiting the activity of AChE would help ameliorate the symptoms of the disease. Acetylcholinesterase inhibitors (AChEIs) such as donepezil, rivastigmine and galantamine have been approved for for the symptomatic treatment of AD. [1]

Choline is an essential nutrient for humans and to maintain health, it must be obtained from the diet as choline or as choline phospholipids, like phosphatidylcholine. Choline is necessary for the synthesis of acetylcholine in the central nervous system. Neurons get their choline from blood circulation by specific protein transporters known as choline transporters which allow the cationic choline to pass through the blood brain barrier (BBB), which is normally impervious to charged species. A gene variation of hChT fairly common in Asians which is known to affect choline uptake may have important implications for the diet requirements of Asians. [2]

The choline transporter (ChT) (SLC5A7) is a cell membrane transporter that carries choline into acetylcholine-synthesizing neurons. In the human brain microvascular endothelial cells of the BBB, two transport systems initiate the choline uptake: (a) the choline transporter-like protein 1, CTL1 (SLC44A1), and (b) the choline transporter-like protein 2, CTL2 (SLC44A2). CTL1 is the primary protein for choline uptake from the extracellular medium. CTL1 is a pH dependent protein, with choline absorption by CTL1 decreasing strongly as the pH becomes more acidic. Choline uptake is also influenced by the electronegativity of the plasma membrane. When the concentration of K^+ ions is increased, the membrane becomes depolarized. The choline absorption decreases primarily as a result of the membrane depolarization by the K^+ ions. Choline uptake by the CTL1 is only affected by the K^+ ions not Na^+ ions. Unlike CTL1 or CTL2, high affinity uptake by ChT is Na^+ dependent, and is also inhibited by hemicholinium-3 which can be used to deplete acetylcholine stores. CTL2 is the main protein involved in the absorption of choline into the mitochondria for its oxidation. [2,3]

A third group of choline transporters is the organic cation transporter (OCT) family, which transport various cations *nonspecifically*, in contrast to the choline-specific transport by CHT1 and CTL members. [2]

It is also known that the *efflux* of choline across the BBB via a carrier mediated efflux transporter system (possibly including the ATP binding cassette transporter (eg p-glycoprotein)) may also be a factor in AD pathogenesis. [4]

In so far as ACh plays a critical role in the pathogenesis of AD, then the transport of choline to the neurons in the brain after passage through the BBB via the intermediate affinity CTL1 and CTL2 is the rate determining step. It is known that the high affinity ChT transports choline into neurons at a greater rate than intermediate affinity CTL1 or CTL2 can transport choline across the BBB. [2,5,6]

There have been numerous studies of potential therapeutic inhibitors of the BBB transporters CTL1 or CTL2 and the neuronal transporter ChT. Also the inhibition of AChE has been widely studied. Both of these inhibitory processes have searched for structure activity relationships (SAR) of potential therapeutics to combat AD, and many molecular descriptors have been used to obtain predictive quantitative SAR. [2,5-9]

The binding of inhibitors to AChE is well characterized since the x-ray structures of various configurations of AChE are well established. [10] The hydrolysis catalytic site of AChe is located near the bottom of a deep and narrow gorge, 20Å deep. Its cross section at the narrowest point is substantially smaller than the diameter of the quaternary group of choline, so AChE must undergo substantial ‘‘breathing’’ motions to carry out its catalytic activity. A remarkable feature of the gorge is that it is lined by the phenyl rings of 14 conserved aromatic amino acids which contribute 60% of the total surface area. There is a misnamed ‘anionic’ subsite of the catalytic site (CAS), which makes **π**-cation interactions with the quaternary group of the substrate. There is also a peripheral anionic site (PAS) at the mouth of the gorge, which serves as a relay station for the substrate en route to the active site. The PAS is ca. 14Å from the CAS. Inhibitors can also bind with aromatic residues midway down the gorge via **π**-cation or **π**- **π** stacking. Many second-generation AChE inhibitors for the treatment of Alzheimer disease are compounds that span the CAS and PAS, whereas most first-generation AChE inhibitors bound to the “anionic” site only. Some inhibitors such as Thioflavin T bind only to the PAS. AChE has been shown to accelerate aggregation of the Aβ peptide, a process critical to the progression of AD. This acceleration appears to involve the PAS only. [10]

The mechanism by which substrates are transported down the 20Å gorge of AChE to the active catalytic site at the bottom of the gorge is well known. The active site of AChE comprises 2 subsites, the anionic site and the esteratic subsite. The PAS at the mouth of the gorge serves as a relay station for the substrate en route to the CAS and ultimately to the esteratic subsite, where acetylcholine is hydrolyzed to acetate and choline. The active site gorge has a high negative electrical potential, and the AChE has a very high dipole moment (> 500 D), with the dipole moment vector aligned with the axis of the gorge. The affinity of quaternary ammonium species to **π**- bond with aromatic AChE residues coupled with the electrostatic force is thought to be responsible for the selective accelerated binding of inhibitors within the gorge of AChE. [10,11,12]

The mechanism by which the membrane transporters CTL and ChT work is not known in humans, since x-ray structures of the embedded proteins are not available. The x-ray structure of a bacterial choline transporter with acetylcholine co-crystallized shows **π**-cation interactions to

the quaternary N^+ atom (mainly Trp-N^+ and Tyr-N^+ interactions) in the binding gorge, with an acetyl C=O---HN Asn hydrogen bond). [13][Oswald 2008]

This study aims to examine (a) whether a previously derived linear free energy model successfully applied to drug transport and drug-protein binding processes can also accurately describe the transport of AD drugs across the BBB and to neurones as well as the inhibitory binding to AChE, (b) and if so, what are the molecular properties of the drugs that determine transport and binding processes.

Results

We have previously described a model that has been shown to apply to a wide range of drug transport, binding, metabolic and cytotoxicity properties of cells and tumours (Equation 1). The model is based on establishing linear free energy relationships between the four drug properties and various biological processes. Equation 1 has been previously applied to passive and facilitated diffusion of a wide range of drugs crossing the blood brain barrier, [14] the active competitive transport of tyrosine kinase inhibitors by the hOCT3, OATP1A2 and OCT1 transporters, and cyclin-dependent kinase inhibitors and HIV-1 protease inhibitors. [22] The model also applies to PARP inhibitors, the anti-bacterial and anti-malarial properties of fluoroquinolones, and active organic anion transporter drug membrane transport, and some competitive statin-CYP enzyme binding processes. There is strong independent evidence from the literature that $\Delta G_{desolvation}$, $\Delta G_{lipophilicity}$, the dipole moment and molecular volume are good inherent indicators of the transport or binding ability of drugs. [14-30]

Equation 1:

Transport or Binding or Cytotoxicity = $\Delta G_{desolv,CDS}$ + $\Delta G_{lipo,CDS}$ + Dipole Moment + Molecular Volume

Eq 1 uses the free energy of water desolvation ($\Delta G_{desolv,CDS}$) and the lipophilicity free energy ($\Delta G_{lipo,CDS}$) where CDS represents the non-electrostatic first solvation shell solvent properties. CDS may be a better approximation of the cybotactic environment around the drug approaching or within the protein receptor pocket, or the cell membrane surface or the surface of a drug transporter, than the bulk water environment outside the receptor pocket or cell membrane surface. The CDS includes dispersion, cavitation, and covalent components of hydrogen bonding, hydrophobic effects. Desolvation of water from the drug ($\Delta G_{desolv,CDS}$) before binding in the receptor pocket is required, and hydrophobic interactions between the drug and protein ($\Delta G_{lipo,CDS}$) is a positive contribution to binding. The lipophilicity $\Delta G_{lipo,CDS}$ is calculated from the solvation energy in n-octane or n-octanol. In some biological processes, where biological reduction may be occurring, and the influence of molecular volume is small, the reduction potential (electron affinity) has been included in place of the molecular volume. In other processes, the influence of some of the independent variables is small and can be eliminated to focus on the major determinants of biological activity.

We have recently used this model to develop a predictive model of the transport and efficacy of hypoxia specific cytotoxic analogues of tirapazamine and the effect on the extravascular penetration of tirapazamine into tumours. [15] It was found that the multiparameter model of the diffusion, antiproliferative assays IC_{50} and aerobic and hypoxic clonogenic assays for a wide range of neutral and radical anion forms of tirapazamine (TPZ) analogues showed: (a) extravascular diffusion is governed by the desolvation, lipophilicity, dipole moment and molecular volume, similar to passive and facilitated permeation through the blood brain barrier and other cellular membranes, (b) hypoxic assay properties of the TPZ analogues showed dependencies on the electron affinity, as well as lipophilicity and dipole moment and desolvation, similar to other biological processes involving permeation of cellular membranes, including nuclear membranes, (c) aerobic assay properties were dependent on the almost exclusively on the electron affinity, consistent with electron transfer involving free radicals being the dominant species.

The model (eq 2) has also been recently applied to triple negative breast and ovarian cancers where transient and stable free radicals are involved in the cytotoxic oxidative stress processes. The electron affinity of the various drugs, along with the water desolvation, lipophilicity and dipole moment, has been shown to be an important predictor of cytotoxic efficacy. [14-28] In our recent study of ORAC and CellROX free radical anticancer drugs and oxidative stress in colorectal cancer cells [16,17] we found that eq 2 was also applicable where the electron affinity replaced the (HOMO-LUMO) variable.

The antioxidant capacity (or chemical reactivity) of the drugs can be assessed by the HOMO-LUMO energy gap, since we have recently shown that this gap is linearly related to the LD_{50} toxicity of various drugs which are involved in oxidative stress processes in some cancers. [16,20-21] Eq 2 can then be represented by including the HOMO-LUMO energy gap instead of the molecular volume. In particular, we have recently examined the mechanism and structure activity relationships of lipid peroxidation of cell membranes and brain protection for cerebral ischemia by Edaravone and Edaravone analogs [29] and improved Edaravone delivery to the brain and crossing the blood brain barrier [30] using variants of eq (2)

Equation 2.

$$\textbf{Oxidative Stress or Toxicity} = \Delta G_{desolv,CDS} + \Delta G_{lipo,CDS} + \textbf{Dipole Moment} + (\textbf{HOMO} - \textbf{LUMO})$$

Evaluation methodology

Given the successful transport, binding or cytotoxicity model as described by eq 1 and 2 for wide range of drugs, the method used was to calculate the molecular parameters for the various CTL or CHT transporter substrates or AChE inhibitors: (1) the free energy of water desolvation ($\Delta G_{desolv,CDS}$), (2) the lipophilicity free energy ($\Delta G_{lipo,CDS}$) in n-octane, (3) the dipole moment in water, (4) the molecular volume in water, and (5) or the HOMO, LUMO or HOMO-LUMO energy gap in water. These values are shown in Tables 1-4. These independent variables values have been standardized to similar magnitudes so that the coefficients in the multiple linear

regression equations can be directly compared to gauge the relative magnitudes of sensitivity of these molecular variables.

Stepwise multiple regression was then applied to seek out which drug molecular properties had the largest most significant effect on the CTL and ChT transport binding or AChE inhibitory binding in Tables 1-4. The resultant equations below indicate the most statistically significant relationships found after testing against all independent variables in a stepwise fashion.

(1) Acetylcholinesterase inhibitors

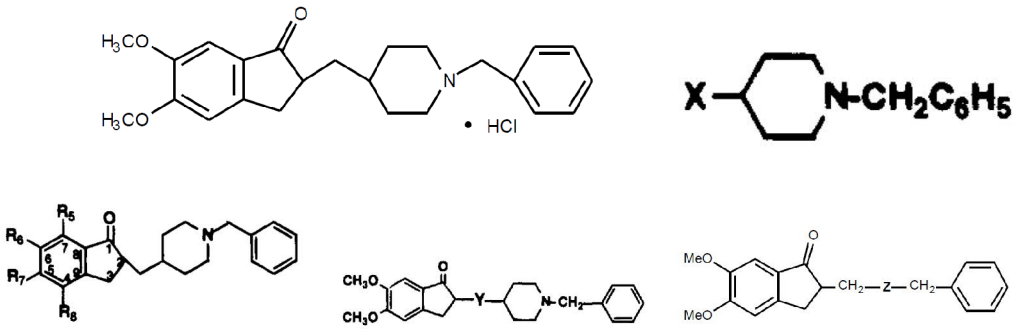

Figure 1 upper left Donepezil, upper right Donepezil analogs with X substituents, lower left with substituents R_5,R_6,R_7,R_8 and lower right, with Y and Z substituents as per Table 1 from Sugimoto 1995 [31].

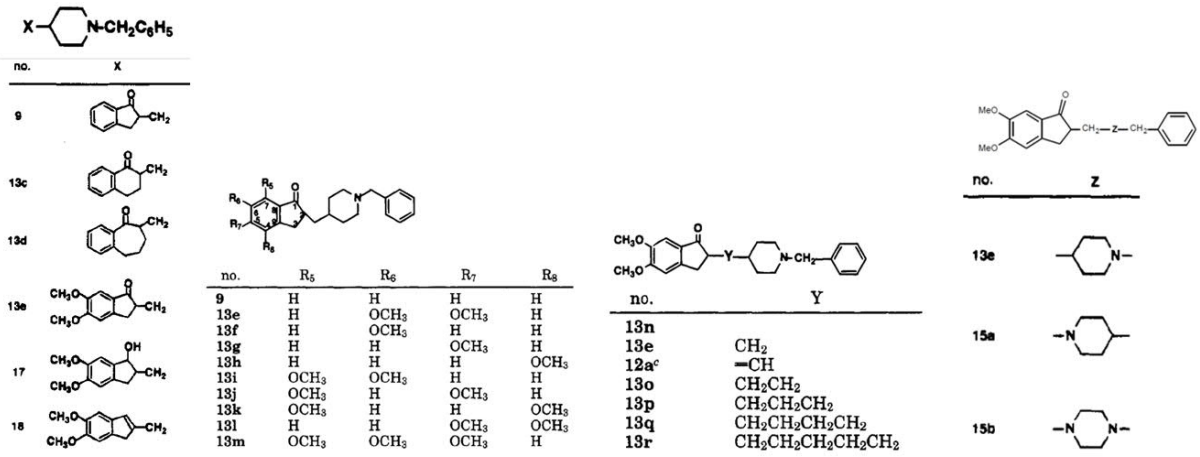

no.	X
9	
13c	
13d	
13e	
17	
18	

no.	R_5	R_6	R_7	R_8
9	H	H	H	H
13e	H	OCH_3	OCH_3	H
13f	H	OCH_3	H	H
13g	H	H	OCH_3	H
13h	H	H	H	OCH_3
13i	OCH_3	OCH_3	H	H
13j	OCH_3	H	OCH_3	H
13k	OCH_3	H	H	OCH_3
13l	H	H	OCH_3	OCH_3
13m	OCH_3	OCH_3	OCH_3	H

no.	Y
13n	
13e	CH_2
12a[c]	=CH
13o	CH_2CH_2
13p	$CH_2CH_2CH_2$
13q	$CH_2CH_2CH_2CH_2$
13r	$CH_2CH_2CH_2CH_2CH_2$

no.	Z
13e	
15a	
15b	

Table 1. Donepezil analogs with X,Y,Z and R_5,R_6,R_7,R_8 substituents as per Table 1 from Sugimoto 1995 [31]

3(a) Donepezil 26 analogs for XYZ and R_5,R_6,R_7,R_8 substituents as per Figure 1, Table1 [Sugimoto 1995][31]

Eq 3(a) Inhibition of AChE for 26 Donepezil analogs from [Sugimoto 1995][31] was:

$$\mathbf{IC_{50} = 16.69\Delta G_{desolv,CDS} + 1134.04\Delta G_{lipo,CDS} - 9.62 Dipole\ Moment + 23291 LUMO + 12945}$$

Where R^2 = 0.670, SEE = 754.9, SE($\Delta G_{desolvCDS}$) = 38.89, SE($\Delta G_{lipoCDS}$) = 1762.2, SE(Dipole Moment) =6.4, SE(LUMO)= 62237, F=10.64, Significance=0.00000

No dependencies were found for molecular volume, HOMO, or HOMO-LUMO for the 26 analogs, but a particularly poor correlation was found in eq 3(a) for LUMO (t stat significance 0.712).

Subdividing all 26 analogs into 2 data base with XYZ substituents and R_5,R_6,R_7,R_8 substituents as per Table 1 allows the close investigation of structural and chain lengthening effects with the XYZ substituents, and separately allowing investigation of purely electronic effects with the R_5,R_6,R_7,R_8 substituents with no major structural influences.

Eq 3(b) Inhibition of AChE for 16 Donepezil analogs with XYZ substituents from Sugimoto 1995][31][was:

$$\mathbf{IC_{50} = 764.0\Delta G_{desolv,CDS} + 845.3\Delta G_{lipo,CDS} - 7.2 Dipole\ Moment - 209114 LUMO + 16289}$$

Where R^2 = 0.827, SEE = 733.3, SE($\Delta G_{desolvCDS}$) = 388,7, SE($\Delta G_{lipoCDS}$) = 260.2, SE(Dipole Moment) =6.4, SE(LUMO)= 149044, F=13.11, Significance=0.00035

Eq 3(c) Inhibition of AChE for 10 Donepezil analogs with R_5,R_6,R_7,R_8 substituents analogs from [Sugimoto 1995][31] was:

$$\mathbf{IC_{50} = -6.26\Delta G_{desolv,CDS} - 81.9\Delta G_{lipo,CDS} + 7.3 Dipole\ Moment - 115287 LUMO - 3537}$$

Where R^2 = 0.818, SEE = 27.0, SE($\Delta G_{desolvCDS}$) = 1.89, SE($\Delta G_{lipoCDS}$) = 25.79, SE(Dipole Moment) =2.3, SE(LUMO) = 34065, F=5.62, Significance=0.043

The separation of the total data base into eq 3(b) and 3(c) gives far stronger correlations than the using the single total data base eq 3(a), particularly the poor correlation with LUMO (t stat significance 0.712). Eq 3(b) shows that inhibition of AChE by the various XYZ Donepezil analogues is most strongly dependent on LUMO (t stat 0.188) with minor dependencies on $\Delta G_{lipo,CDS}$ and $\Delta G_{desolv,CDS}$, and negligible dependencies on dipole moment. Eq 3(c) for the R_5,R_6,R_7,R_8 substituents is most strongly dependent on LUMO (t stat 0.019) with virtually no major dependency on other variables. These results indicate that there are two major influences for the inhibitory effect of donepezil analogs on AChE: firstly a structural steric effect related to the length of the inhibitors, with some minor steric effect for the R(N^+) moiety, and the associated influence of the LUMO's of the inhibitors, and secondly, a mainly electronic effect related to the LUMO of the inhibitor and its interaction with the HOMO of AChE in the binding interaction.

(a) TAK-147 (3-[1-(phenylmethyl)-4-piperidinyl]-1-(2,3,4,5-tetrahydro-1H-1-benzazepin-8-yl)-1-propanone fumarate) analogs [Ishihara 2000][32]

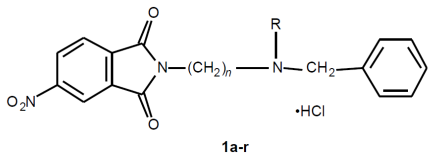

1a-r

Figure 2(a). TAK-147 inhibitors of AChE with (n) increasing chain lengths and various N^+-R substituents (see Table 2 for R groups) from Ishihara 2000 [32]

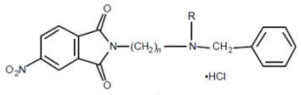

1a-r

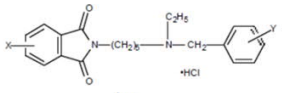

1s-cc

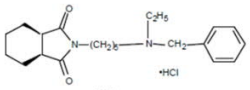

1dd

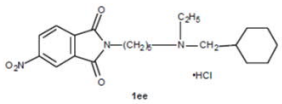

1ee

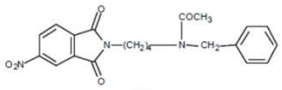

1ff

Compd.	n	R	IC_{50} (nM)
1a	3	Me	93600
1b	4	Me	8320
1c	5	Me	1360
1d	6	Me	474
1e	7	Me	1780
1f	8	Me	8250
1g	9	Me	27900
1h	3	Et	12300
1i	4	Et	252
1j	5	Et	151
1k	6	Et	607
1l	7	Et	4530
1m	3	*iso*-Pr	56200
1n	4	*iso*-Pr	495
1o	5	*iso*-Pr	824
1p	3	Pr	44000
1q	4	Pr	1870
1r	5	Pr	2650

Compd.	X	Y	IC_{50} (nM)
1s	H	H	3370
1t	4-NO_2	H	637
1u	5-Me	H	1750
1v	5-Cl	H	1330
1w	5-OMe	H	701
1x	5-NHAc	H	328
1y	5-CONHMe	H	380
1z	5-NO_2	2-OMe	23.9
1aa	5-NO_2	3-OMe	44.8
1bb	5-NO_2	4-OMe	269
1cc	5-NO_2	3-OCONHMe	0.380
1dd	-	-	18500
1ee	-	-	1090
1ff	-	-	> 100000

Table 2. TAK-147 inhibitors of AChE with (n) increasing chain lengths and various N^+-R substituents, and constant chain lengths and N^+-Ethyl substituents, as per Figures 2(a) and 2(b) from Ishihara 2000 [32]

Eq 4(a) Inhibition of AChE for 18 TAK-147 analogs substituted at N^+(R) and increasing chain length (see Figure 2(a)) from [Ishihara 2000][32] was:

$$\mathbf{IC_{50} = -540.20\Delta G_{desolv,CDS} + 1593.4\Delta G_{lipo,CDS} - 4816.3Volume - 407522LUMO - 3396511}$$

Where R^2 = 0.544, SEE = 19616.4, SE($\Delta G_{desolvCDS}$) = 9887.6, SE($\Delta G_{lipoCDS}$) = 2354.6 SE(Volume) =4060, SE(LUMO) = 151005, F=3.88, Significance=0.0274

It is clear from eq 4(a) that IC_{50} is not strongly correlated with $\Delta G_{desolv,CDS}$ or $\Delta G_{lipo,CDS}$, and shows a weak dependency on Molecular Volume, but is strongly correlated with the LUMO of the inhibitors. See eq 4(b) below.

Eq 4(b) Inhibition of AChE for 18 TAK-147 analogs substituted at N^+(R) and increasing chain length (see Figure 2(a)) from [Ishihara 2000][32] was:

$$\mathbf{IC_{50} = -4660.4Volume + 440841LUMO - 3694803}$$

Where R^2 = 0.528, SEE = 18581.7, SE(Volume) =3321, SE(LUMO) = 133989, F=8.40, Significance=0.0035

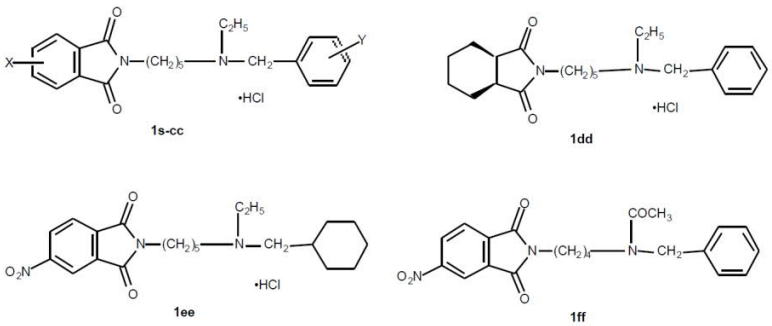

Figure 2(b). TAK-147 inhibitors of AChE with constant chain lengths and N^+-Ethyl substituents (see Table 2 for X,Y groups) from Ishihara 2000 [32]

Analysis of a series of 13 TAK-147 analogs where the cationic quaternary N atom has a constant ethyl substituent (see Figure 2(b)) allows an investigation of the effect of molecular properties on IC_{50} activity. It was found that there was no correlation with $\Delta G_{lipo,CDS}$**,** Molecular Volume, HOMO, HOMO-LUMO, but correlations with LUMO in particular, and weaker correlations with dipole moment and $\Delta G_{desolv,CDS}$, resulting in eq 4(c) below:

Eq 4(c) Inhibition of AChE for 13 TAK-147 analogs with a constant N^+(Ethyl) framework(see Figure 2(b)) from [Ishihara 2000][32] was:

$$\mathbf{IC_{50} = -433.7\Delta G_{desolv,CDS} + 306.1 Dipole\ Moment + 45081.4 LUMO + 6656.8}$$

Where R^2 = 0.889, SEE = 1919.6, SE($\Delta G_{desolvCDS}$) = 603.8, SE(DM) = 155.7, SE(LUMO) = 6384.7, F=24.02, Significance=0.0001

Eliminating the poorly correlated $\Delta G_{desolv,CDS}$ results in eq 4(d) which illustrates inhibitory activity is very strongly correlated with LUMO with a minor dependence on dipole moment.

Eq 4(d) Inhibition of AChE for 13 TAK-147 analogs with a constant N^+(Ethyl) framework(see Figure 2(b)) from [Ishihara 2000][32] was:

$$\mathbf{IC_{50} = 391.1 Dipole\ Moment + 42448.5 LUMO + 6844.4}$$

Where R^2 = 0.882, SEE = 1872.5, SE(DM) = 113.1, SE(LUMO) = 5098.5, F=37.60, Significance=0.00002

It is noted that a multilinear analysis of IC_{50} for the 31 analogs 1a-1r and 1s-1cc plus 1dd and 1ee (Table 2) gave a very poor correlation against all variables, whereas subdividing the data sets as shown in Figures 2(a) and 2(b) gave strong correlations as finally shown in eq 4(b) and 4(d). These results are similar to those for the Donepezil analogs where firstly a structural steric effect related to the length of the inhibitors, with some minor steric effect for the R(N^+) moiety, and the associated influence of the LUMO's of the inhibitors, and secondly, a mainly electronic effect (where structural features are kept constant) related to the LUMO of the inhibitor and its interaction with the HOMO of AChE in the binding interaction.

It is noted that eq 4(b) can explain the unusual observation where increasing the molecular length (and volume) see Table 2, 1a-1r, gradually increasing the binding, but then reaches a maximum, and then starts to decrease as the inhibitor further increases in length. While molecular volume is significant in eq 4(b), the dominant influence is still the LUMO.

(2) BBB Choline Transporter (CTL) of cationic substrates

See Figure 3 for CTL inhibitor structures.

Eq 5(a) Transport of 24 cationic substrates by CTL[Geldenhuys 2010][9], (3 outliers 6,8,19):

$$\mathbf{LogKi = 0.016\Delta G_{desolv,CDS} + 0.154\Delta G_{lipo,CDS} - 0.09Dipole\ Moment - 0.07HOMO + 5.09}$$

Where R^2 = 0.603, SEE = 0.402, SE($\Delta G_{desolvCDS}$) = 0.026, SE($\Delta G_{lipoCDS}$) = 0.060, SE(Dipole Moment) =0.022, SE(HOMO) = 0.085, F=7.20, Significance=0.0010

Linear correlations between LogKi and $\Delta G_{desolv,CDS}$, $\Delta G_{lipo,CDS}$, Dipole Moment and HOMO were individually strong, and were incorporated into eq 5(a). Also linear correlations between LogKi and LUMO and molecular volume in water were poor. It can be seen from the multi-linear eq 5(a) that the correlation with $\Delta G_{desolv,CDS}$ is poor compared to $\Delta G_{lipo,CDS}$, DM and HOMO and can be discarded to give eq 5(b). Eq 5(b) indicates that logKi is most strongly dependent on lipophilicity, and then equally dependent on dipole moment and HOMO at half that of lipophilicity.

Eq 5(b) Transport of 24 cationic substrates across BBB by CTL Transporters [Geldenhuys 2010][9]:

$$\mathbf{LogKi = 0.176\Delta G_{lipo,CDS} - 0.094Dipole\ Moment - 0.092HOMO + 5.53}$$

Where R^2 = 0.595, SEE = 0.395, SE($\Delta G_{lipoCDS}$) = 0.047, SE(Dipole Moment) =0.020, SE(HOMO) = 0.076, F=9.80, Significance=0.0003

(3) Neuronal choline transporter (ChT) of cationic substrates

See Figure 4 or ChT inhibitor structures.

Eq 6(a) Transport of 39 cationic substrates by ChT [Geldenhuys 2010][33]:

$$\mathbf{LogKi = -0.112\Delta G_{desolv,CDS} - 0.313\Delta G_{lipo,CDS} - 0.042DM - 0.022Volume - 0.421HOMO + 6.23}$$

Where R^2 = 0.555, SEE = 1.183, SE($\Delta G_{desolvCDS}$) = 0.127, SE($\Delta G_{lipoCDS}$) = 0.222, SE(Dipole Moment) =0.068, SE(Volume) = 0.09, SE(HOMO) = 0.197, F=7.20, Significance=0.0010

It can be seen from the multi-linear eq 6(a) that there is no significant correlation with logKi for the dipole moment (DM) or molecular volume (Volume) in water, despite there being strong individual linear correlations between LogKi and DM, Volume. The correlation is strongest between logKi and $\Delta G_{desolv,CDS}$, $\Delta G_{lipo,CDS,}$ and HOMO. The correlation between LogKi and HOMO is the strongest of all the individual correlations, followed by $\Delta G_{lipo,CDS}$, then $\Delta G_{desolv,CDS}$

as shown in eq 6(b), then 6(c), and finally 6(d). It is also noted that the correlation of LogKi with LUMO was very poor.

Eq 6(b) Transport of 39 cationic substrates by ChT [Geldenhuys 2010][33]:

$$\mathbf{pKi = -0.065\Delta G_{desolv,CDS} - 0.242\Delta G_{lipo,CDS} + 0.388HOMO + 6.06}$$

Where R^2 = 0.550, SEE = 1.155, SE($\Delta G_{desolvCDS}$) = 0.080, SE($\Delta G_{lipoCDS}$) = 0.103, SE(HOMO) = 0.185, F=14.23, Significance=0.00000

Eq 6(c) Transport of 39 cationic substrates by ChT [Geldenhuys 2010][34]:

$$\mathbf{pKi = -0.271\Delta G_{lipo,CDS} + 0.444HOMO + 6.78}$$

Where R^2 = 0.541, SEE = 1.150, SE($\Delta G_{lipoCDS}$) = 0.095, SE(HOMO) = 0.171, F=21.24, Significance=0.000000

Eq 6(d) Transport of 39 cationic substrates by ChT [Geldenhuys 2010][34]:

$$\mathbf{pKi = 0.760HOMO + 10.36}$$

Where R^2 = 0.439, SEE = 1.254, SE(HOMO) = 0.141, F=28.92, Significance=0.000000

Discussion

Acetylcholinesterase inhibitors

The X-ray structure of the Donepezil-*Tc*AChE complex shows that Donepezil has a unique orientation along the active-site gorge, extending from the anionic subsite of the active site (CAS), at the bottom, to the peripheral anionic site (PAS), at the top, via aromatic stacking interactions with conserved aromatic acid residues. Donepezil does not, however, interact directly with either the catalytic triad or the 'oxyanion hole' but only indirectly via solvent molecules. It has been recently shown that docking studies of inhibitor-AChE interactions using the naked AChE structure can be misleading since the conditions used to obtain crystals can give quite different results, and highly conserved water molecules may be involved in inhibitor-AChE binding which may not be accounted for in docking studies. [34,35][Kryger 1999, Silman 2017]

The most striking result from the inhibitor analysis of the donepezil and TAK-147 analogs with AChE is the unexpected strong dependency on the LUMO, as well as the expected dependencies on inhibitor lipophilicity, water desolvation, and dipole moment as shown in eq 3(c) for the donepezil analogs where lipophilicity and water desolvation are the dominant variables. However these analogs include a very wide range of substituents, with varying chain length and varying substituents on N^+.

Caliandro 2018 [36] has shown that desolvation of the donepezil analog inhibitors in the AChE gorge is an important aspect of the binding process.

When the TAK-147 results are split into two discrete data bases, ie firstly with increasing chain lengths and various N^+-R substituents, and then secondly with constant chain lengths and N^+-

ethyl substituents: (a) then it emerges from eq 4(b) that the dominant molecular property is the LUMO, with a much lesser dependency on molecular volume. The molecular volume dependency can explain the unusual observation that inhibition of AChE by inhibitors where R-N^+ is constant, but the methylene group spacers are increased in length, an optimum binding point is reached as the number of spacer groups is increased, then the binding decreases with additional spacers (see Table 2, 1a-1r, and Figure 2(a). Thus eq 4(b) is consistent with a binding mechanism that requires an optimum lengthwise steric interaction and to a lesser extent a steric interaction on the tertiary N^+ atom in the binding gorge of AChE. It is not clear that Ishihara's 2000 docking studies can adequately account for this effect; [15] (b) eq 4(d) for constant chain lengths and N^+-ethyl substituents, it is shown that the LUMO is the strongly dominant variable with a much weaker dependency on dipole moment. It appears that steric effects from increasing length beyond a certain point and steric interactions at the R-N^+ location can lower the binding interaction of the inhibitors which are largely manifest in the LUMO. This result is consistent with the known mechanism for AChE inhibition.

The molecular origin of the very high rate of AChE catalysis is known. Ripoll 1993 [11] utilized the X-ray structure of *Torpedo californica* AChE to calculate the electric field of the AChE and found that the hemisphere of AChE that contains the active site gorge has a high negative electrical potential, and that the overall protein has a dipole moment of greater than 500 D, with the dipole moment vector aligned with the axis of the gorge. This alignment results in cationic species being drawn to the active site by the electrostatic charge. Within the gorge, aromatic amino acid residues shield the cationic species from the negatively charged residues that give AChE its high dipole moment. The affinity of quaternary ammonium species to $\boldsymbol{\pi}$- bond with aromatic residues coupled with the electrostatic force is thought to be responsible for the selective binding of inhibitors with the gorge of AChE. This electric field accelerates the binding of positive charged quaternary ammonium ligands to the enzyme. [11,12]

Eq 4(c) indicates that it is the $\boldsymbol{\pi}$- binding at the active site of the gorge that results in electron transfer from the HOMO of AChE to the LUMO of the inhibitors that dominates when the inhibitor is located in the binding gorge. The dipole moment of the inhibitor is also important in the binding gorge, and presumably even of greater importance as the inhibitor enters the gorge. Other variable such as desolvation, lipophilicity and volume would be expected to be important at this earlier stage, as shown in eq 4(a).

Ruark 2013 [37] developed a QSAR model of pentavalent organophosphate oxon human acetylcholinesterase bimolecular rate constants from a literature database of 278 three-dimensional structures and their bimolecular rates. This database was tested against 675 molecular descriptors, and it was found that the HOMO-LUMO energy gap contributed most significantly to the binding affinity. Ruark's results may have not been conducted in water solvent, unlike this study. Another problem with Ruark's results is that a wide range of

experimental conditions were used for the various literature studies, so the experimental rate constants have varying errors across the different laboratories, which can be avoided in the experimental studies used here since the data comes from the same laboratory for each of the four data sets. However, eq 4(c) does not show any dependency on HOMO or the HOMO-LUMO energy gap, but shows a strong correlation with the LUMO.

BBB Choline Transporter (CTL) of cationic substrates

The delivery of charged drugs to the brain is severely hindered by the fact that charged species do not passively cross the BBB, so other means such as the use of transporters may be used. The BBB choline transporter (CTL) is considered to be a suitable vector for the CNS delivery of cationic drugs, since choline plasma concentrations are only ca 25% of the K_m of that for choline at the BBB CTL. So the CTL has spare capacity to transport other drugs without interrupting the vital supply of choline to the CNS.

Transporters such as the BBB CTL and neuronal ChT are polytopic membrane proteins, and difficult to crystallize, so no X-ray crystal structures of these human transporters are available. It is known that intermediate affinity CTL and high affinity ChT transporters are kinetically different, despite having significant overlapping ability to bind cationic species. The x-ray structure of a bacterial choline transporter with acetylcholine co-crystallized shows $\boldsymbol{\pi}$-cation interactions to the quaternary N^+ atom (mainly $\boldsymbol{\pi}$-Trp-N^+ and $\boldsymbol{\pi}$-Tyr-N^+ interactions) in the binding gorge or pore, with an acetyl C=O---HN Asn hydrogen bond). Figure 5(a) shows a schematic view of how the bacterial ChT transports choline. [13] This $\boldsymbol{\pi}$-binding arrangement to the cationic quaternary N^+ is similar but less comprehensive to that found in the substrate binding at the PAS and CAS of AChE. However the transport of substrates down the gorge of AChE is known to be electrostatically enhanced as a result of the very large dipole moment that points down the gorge of AChE. [11,12] Such a large dipole cannot exist in proteins embedded in membranes, such as the CTL and ChT transporters.

Kinetic studies of the CTL transport of cationic species indicate that (a) there are two anionic sites on the CTL transporters, one of which binds to choline, (b) the presence of a hydroxyl near one of the anionic sites can promote higher affinity (as with choline), but since some bi-cationic species without a hydroxyl group have high affinities, then a hydroxyl group is not a mandatory requirement, and the second anionic site distally removed from the anionic site which binds choline, is an important secondary binding site for bi-cationic species(c) hydrophobic groups adjacent to the cationic N atom of drug increase binding affinities for the CTL transporters, indicating that hydrophobic regions adjacent to anionic sites on the transporter are important. The well characterized ChT inhibitor hemicholinium-3 has two quaternary N^+ sites separated by ca 14Å. By comparison it is interesting to note that PAS is also ca 14Å from the CAS in the binding gorge of AChE. [9,33,38] Figure 5(b) illustrates schematically how the ChT transporter can transport a di-cationic substrate.

It is clear that the CTL and ChT membrane transporters share very similar structural and kinetic features to the binding gorge of AChE. The similarity between enzymes and active membrane transporters has been investigated, noting that these active transporters can catalyze transport

across a membrane by coupling solute movement to a source of energy such as ATP or a secondary ion gradient. It is thought that the transport process and associated energetic coupling involve molecular conformational changes in the transporter. Transportation involves binding interactions that selectively stabilize the higher energy conformations, hence promoting conformational changes in the system that are coupled to decreases in free energy and substrate translocation. [39] However the *transport of substrates down the AChE gorge is accelerated by the large dipole moment orientated down the gorge, which is absent in the CTL and ChT transporters*.

Eq 5(a) and (b) show that LogKi of cationic substrates is mainly dependent on lipophilicity and dipole moment and HOMO each by extent of half that of lipophilicity. Compared to the results for the AChE inhibition discussed above, and while AChE is a free enzyme and CTL are membrane transporters as shown in Figures 5(a) and (b), the primary difference in results is that CTL substrates are dependent on the HOMO whereas the AChE inhibitors are dependent on the LUMO. This may be attributed to the fact that the inhibition of AChE is a binding process facilitated by electron transfer from the HOMO of the AChE to the LUMO of the cationic inhibitors, whereas the transportation of cationic species by the CTL transporter does not involve such a strong binding process, more a weaker interaction involving electron transfer from the HOMO of the substrates to the LUMO of the transporters that ultimately allows the passage through the CTL pore. Assuming that it is a conformational change in the CTL that drives the transport process through the membrane pore, then a substrate HOMO → CTL LUMO interaction seems plausible.

Neuronal choline transporter (ChT) of cationic substrates

The choline uptake activity of CTL1 is distinct from that of CHT1 as regards with the affinity for choline (intermediate versus high), CTL1 is independent on Na^+ whereas CHT1 is dependent on Na^+, and inhibition of CTL1 by HC-3 has a high Ki whereas inhibition of ChT1 by HC-3 has a low Ki. It is thought that hChT1 high-affinity choline uptake activity is performed by a single protein of ChT1 or its oligomer, and has 13 trans-membrane segments, and that amino acid residues with a pKa of 7.4 are involved in uptake activity. [2]

It is known that extracellular choline rapidly decreases cell-surface CHT1 expression by accelerating its internalization, a process that is mediated by a dynamin-dependent endocytosis pathway. The inhibitor hemicholinium-3 decreases the internalization rate and increases cell-surface ChT1 expression. Internalization of ChT1 also depends on extracellular pH. Internalization of ChT1 is induced by extracellular substrate, providing a novel feedback mechanism for the regulation of acetylcholine synthesis at the cholinergic presynaptic terminals. [23]

Eq 6(a) to (d) clearly illustrate that neuronal transport of cationic substrates is predominantly governed by the HOMO, with lesser dependencies on the desolvation and lipophilicity, and

much weaker dependencies on dipole moment and volume. The dependency on HOMO is much stronger than that for the CTL transporter, as expected for the high affinity ChT versus intermediate affinity CTL transporter. This is consistent with a substrate HOMO → ChT LUMO interaction which may subsequently result in a conformational change in the ChT that drives the transport process through the membrane pore, similarly to the for the CTL transporter.

Conclusions

It has been shown that there are similarities between the transport of potential cationic Alzheimer's disease drugs across the blood brain barrier and into neurons compared to the inhibitory binding of acetylcholinesterase. An analysis of water desolvation, lipophilicity, dipole moment, molecular volume, HOMO, LUMO or HOMO-LUMO molecular properties and their impact on transport or inhibitory binding has shown that while lipophilicity, dipole moment, desolvation, and molecular volume are important but varying determinants for transport and inhibitory binding, the HOMO is the important determinant for transport processes, but the LUMO is the more important determinant for the inhibitory binding to acetylcholinesterase. This difference appears to be a general consequence of the higher $\boldsymbol{\pi}$-cation interaction in the binding gorge of acetylcholinesterase compared to the weaker $\boldsymbol{\pi}$-cation and hydrophobic interaction of substrates in the pore of the CTL or ChT transporters. Inhibition of AChE is a binding process facilitated by electron transfer from the HOMO of the AChE to the LUMO of the cationic inhibitors, whereas the transportation of cationic species by the CTL and ChT transporters does not involve such a strong binding process, but more a weaker interaction involving electron transfer from the HOMO of the substrates to the LUMO of the transporters that ultimately allows the passage of substrates through the CTL and ChT pores. There is supporting but not explicit evidence in the literature that points to the similarities between the transport of drugs through the blood brain barrier or into neurons when compared to the binding of cationic drugs to acetylcholinesterase.

An analysis of the molecular volumes of the TAK-147 analogs on binding to AChE where the increasing length of the analogs by adding methylene spacing groups leads to an optimum binding interaction with AChE which then decreases with the addition of further spacers is explained by the binding interaction being dependent on the molecular volume and the LUMO.

Experimental Methods

All calculations were carried out using the Gaussian 09 package. Energy optimizations were at the DFT/B3LYP/6-31G(d,p) (6d, 7f) or DFT/B3LYP/3-21G (for larger molecules) level of theory for all atoms. Selected optimizations at the DFT/B3LYP/6-311+G(d,p) (6d, 7f) level of theory gave very similar results to those at the lower level. Optimized structures were checked to ensure energy minima were located, with no imaginary frequencies. Energy calculations were conducted at the DFT/B3LYP/6-31G(d,p) (6d, 7f) for neutral and cationic compounds with

optimized geometries in water, using the IEFPCM/SMD solvent model. With the 6-31G* basis set, the SMD model achieves mean unsigned errors of 0.6 - 1.0 kcal/mol in the solvation free energies of tested neutrals and mean unsigned errors of 4 kcal/mol on average for ions. [41] The 6-31G** basis set has been used to calculate absolute free energies of solvation and compare these data with experimental results for more than 500 neutral and charged compounds. The calculated values were in good agreement with experimental results across a wide range of compounds. [42,43] Adding diffuse functions to the 6-31G* basis set (ie 6-31+G**) had no significant effect on the solvation energies with a difference of less than 1% observed in solvents, which is within the literature error range for the IEFPCM/SMD solvent model. HOMO and LUMO calculations included both delocalized and localized orbitals (NBO).

It is noted that high computational accuracy for each species in different environments is not the focus of this study, but comparative differences between various species is the aim of the study. The errors in the experimental pKi, logKi or IC_{50} values far exceed those errors in the molecular properties calculated by quantum mechanics.

References

[1] K Sharma, Cholinesterase inhibitors as Alzheimer's therapeutics (Review), Mol Med Reports, 2019, 20, 1479-1487

[2] T Haga, Molecular properties of the high-affinity choline transporter CHT1, J. Biochem. 2014, 156, 181–194

[3] M Inazu, Functional Expression of Choline Transporters in the Blood–Brain Barrier, Nutrients, 2019, 11, 2265-2274

[4] NY Lee, YS Kang, The Efflux Transport of Choline through Blood-Brain Barrier is Inhibited by Alzheimer's Disease Therapeutics, Biomolec Therapeutics, 2008, 16, 179-183

[5] WJ Geldenhuys, VK Manda, RK Mittapalli, CJ Van der Schyf, PA Crooks, LP Dwoskin, DD Allen, PR Lockman, Predictive Screening Model for Potential Vector-Mediated Transport of Cationic Substrates at the Blood-Brain Barrier Choline Transporter, Bioorg Med Chem Lett. 2010, 20, 870-892

[6] DD Allen, QR Smith, Characterization of the blood brain barrier choline transporter using the in situ rat brain perfusion technique, J Neurochem, 2001, 76, 1032-1041

[7] H Murakami, N Sawada, N Koyabu, H Ohtani, Y Sawada, Characteristics of Choline Transport Across the Blood-Brain Barrier in Mice: Correlation with In Vitro Data, Pharmaceut Res, 2000, 17, 1526–1530

[8] S Shityakov, C Forster, In silico predictive model to determine vector-mediated transport properties for the blood–brain barrier choline transporter, Adv Appl Bioinformatics Chem, 2014,7, 23-36

[9] W J Geldenhuys, VK Manda, RK Mittapallia, CJ Van der Schyf, PA Crooks, LP Dwoskin, DD Allen, PR Lockman, Predictive Screening Model for Potential Vector-Mediated Transport of Cationic Substrates at the Blood-Brain Barrier Choline Transporter, 2010, 20, 870-892

[10] Y Xu, JP Colletier, M Weik, H Jiang, J Moult, I Silman, JL Sussman, Flexibility of Aromatic Residues in the Active-Site Gorge of Acetylcholinesterase: X-ray versus Molecular Dynamics, Biophy J. 2008, 95, 2500-2511

[11] DR Ripoll, CH Faerman, PH Axelsen, I Silman, JL Sussman An Electrostatic Mechanism for Substrate Guidance Down the Aromatic Gorge of Acetylcholinesterase, PNAS, 1993, 90, 5128-5132

[12]D Porschke, C Créminon, X Cousin, C Bon, J Sussman, I Silman, Electrooptical measurements demonstrate a large permanent dipole moment associated with acetylcholinesterase, 1996, 70, 1603-8
[13] C Oswald,SH Smits, M Hoing, L Sohn-Bosser, L Dupont, D Le Rudulier, L Schmitt, E Bremer, Crystal structures of the choline/acetylcholine substrate-binding protein ChoX from Sinorhizobium meliloti in the liganded and unliganded-closed states, J.Biol.Chem. 2008, 283**,** 32848-32859
[14] CW Fong, Permeability of the Blood–Brain Barrier: Molecular Mechanism of Transport of Drugs and Physiologically Important Compounds, J Membr Biol. 2015, 248,651-69.
[15] CW Fong, The extravascular penetration of tirapazamine into tumours: a predictive model of the transport and efficacy of hypoxia specific cytotoxic analogues and the potential use of cucurbiturils to facilitate delivery, Int J Comput Biol Drug Design. 2017, 10, 343-373
[16] CW Fong, Screening anti-colorectal cancer drugs: free radical chemotherapy, HAL Archives, 2019, https://hal.archives-ouvertes.fr/hal-02271521v1
[17] CW Fong, Free radical anticancer drugs and oxidative stress: ORAC and CellROX-colorectal cancer cells by quantum chemical determinations, HAL Archives, 2018 https://hal.archives-ouvertes.fr/hal-01859315v1.
[18] CW Fong, The role of free radicals in the effectiveness of anti-cancer chemotherapy in hypoxic ovarian cells and tumours, HAL Archives, 2018, hal-01659879, https://hal.archives-ouvertes.fr/hal-01659879v2
[19] CW Fong, Free radicals in chemotherapy induced cytotoxicity and oxidative stress in triple negative breast and ovarian cancers under hypoxic and normoxic conditions, HAL Archives, 2018, https://hal.archives-ouvertes.fr/hal-01815246v1
[20] CW Fong, Role of stable free radicals in conjugated antioxidant and cytotoxicity treatment of triple negative breast cancer, HAL archives 2018, https://hal.archives-ouvertes.fr/hal-01803297
[21] CW Fong, Toxicology of platinum anticancer drugs: oxidative stress and antioxidant effect of stable free radical Pt-nitroxides, HAL Archives, 2019, hal-01999011, version 1**,** https://hal.archives-ouvertes.fr/hal-01999011v1
[22] CW Fong, The effect of desolvation on the binding of inhibitors to HIV-1 protease and cyclin-dependent kinases: Causes of resistance, Bioorg Med Chem Lett. 2016, 26, 3705–3713.
[23] CW Fong, Physiology of ionophore transport of potassium and sodium ions across cell membranes: Valinomycin and 18-Crown-6 Ether. Int J Comput Biol Drug Design 2016, 9, 228-246.
[24] CW Fong, Statins in therapy: Understanding their hydrophilicity, lipophilicity, binding to 3-hydroxy-3-methylglutaryl-CoA reductase, ability to cross the blood brain barrier and metabolic stability based on electrostatic molecular orbital studies. Eur J Med Chem. 2014, 85, 661-674
[25] CW Fong, Predicting PARP inhibitory activity – A novel quantum mechanical based model. HAL Archives. 2016, https://hal.archives-ouvertes.fr/hal-01367894v1.
[26] CW Fong, A novel predictive model for the anti-bacterial, anti-malarial and hERG cardiac QT prolongation properties of fluoroquinolones, HAL Archives. 2016, https://hal.archives-ouvertes.fr/hal-01363812v1.
[27] CW Fong, Statins in therapy: Cellular transport, side effects, drug-drug interactions and cytotoxicity - the unrecognized role of lactones, HAL Archives, 2016, https://hal.archives-ouvertes.fr/hal-01185910v1.
[28] CW Fong, Drug discovery model using molecular orbital computations: tyrosine kinase inhibitors. HAL Archives, 2016, https://hal.archives-ouvertes.fr/hal-01350862v1
[29] CW Fong, Mechanism, structure activity relationships of lipid peroxidation of cell membranes and brain protection for cerebral ischemia by Edaravone and Edaravone analogs – a quantum mechanical study, HAL Archives, 2019, hal-02428109, https://hal.archives-ouvertes.fr/hal-02428109v1
[30] CW Fong, Improved Edaravone delivery to the brain and crossing the blood brain barrier: using quantum mechanics, HAL Archives, 2019, hal-02292553v2, https://hal.archives-ouvertes.fr/hal-02292553v2

[31] H Sugimoto, Y Yamanishi, Y Iimura, Y Kawakami, Donepezil Hydrochloride (E2020) and Other Acetylcholinesterase Inhibitors, Curr Med Chem, 2000, 7, 303-339
[32] Y Ishihara, G Goto M Miyamoto, Central Selective Acetylcholinesterase Inhibitor with Neurotrophic Activity: Structure-Activity Relationships of TAK-147 and Related Compounds, Curr Med Chem, 2000, 7, 341-354
[33] WJ Geldenhuys, DD. Allen, PR Lockman 3-D-QSAR and docking studies on the neuronal choline transporter, Bioorg Med Chem Lett 2010, 20, 4870–4877
[34] G Kryger, I Silman, JL Sussman, Structure of acetylcholinesterase complexed with E2020 (Aricept): implications for the design of new anti-Alzheimer drugs, Structure 1999, 15, 297-307
[35] I Silman, JL Sussman, Recent developments in structural studies of acetylcholinesterase, J Neurochem, 2017, 142(Suppl 2), 19-25
[36] R Caliandro, A Pesaresi, L Cariati, A Procopio, M Oliverio, D Lamba, Kinetic and structural studies on the interactions of Torpedo californica acetylcholinesterase with two donepezil-like rigid analogues, J Enz Inhib Med Chem, 2018, 33, 794-803
[37] CD Ruark, CE Hack, PJ Robinson, PE Anderson, JM Gearhart, Quantitative structure-activity relationships for organophosphates binding to acetylcholinesterase, Arch Toxicol. 2013, 87, 281-9.
[38] WJ Geldenhuys, AS Mohammad, CE Adkins, PR Lockman, Molecular determinants of blood–brain barrier permeation, Ther. Deliv. 2015, 6, 961–971
[39]BH Shilton, Active transporters as enzymes: an energetic framework applied to major facilitator superfamily and ABC importer systems, Biochem J, 2015, 467,193-9
[40] T Okuda,A Konishi, H Misawa, T Haga, Substrate-Induced Internalization of the High-Affinity Choline Transporter, J Neorosci, 2011, 31,14989-14997
[41] AV Marenich, CJ Cramer, DJ Truhlar, Universal Solvation Model Based on Solute Electron Density and on a Continuum Model of the Solvent Defined by the Bulk Dielectric Constant and Atomic Surface Tensions, J Phys Chem B, 2009, 113, 6378 -96
[42] S Rayne, K Forest, Accuracy of computational solvation free energies for neutral and ionic compounds: Dependence on level of theory and solvent model, Nature Proceedings, 2010, http://dx.doi.org/10.1038/npre.2010.4864.1.
[43] RC Rizzo, T Aynechi, DA Case, ID Kuntz, Estimation of Absolute Free Energies of Hydration Using Continuum Methods: Accuracy of Partial Charge Models and Optimization of Nonpolar Contributions, J Chem Theory Comput. 2006, 2, 128-139

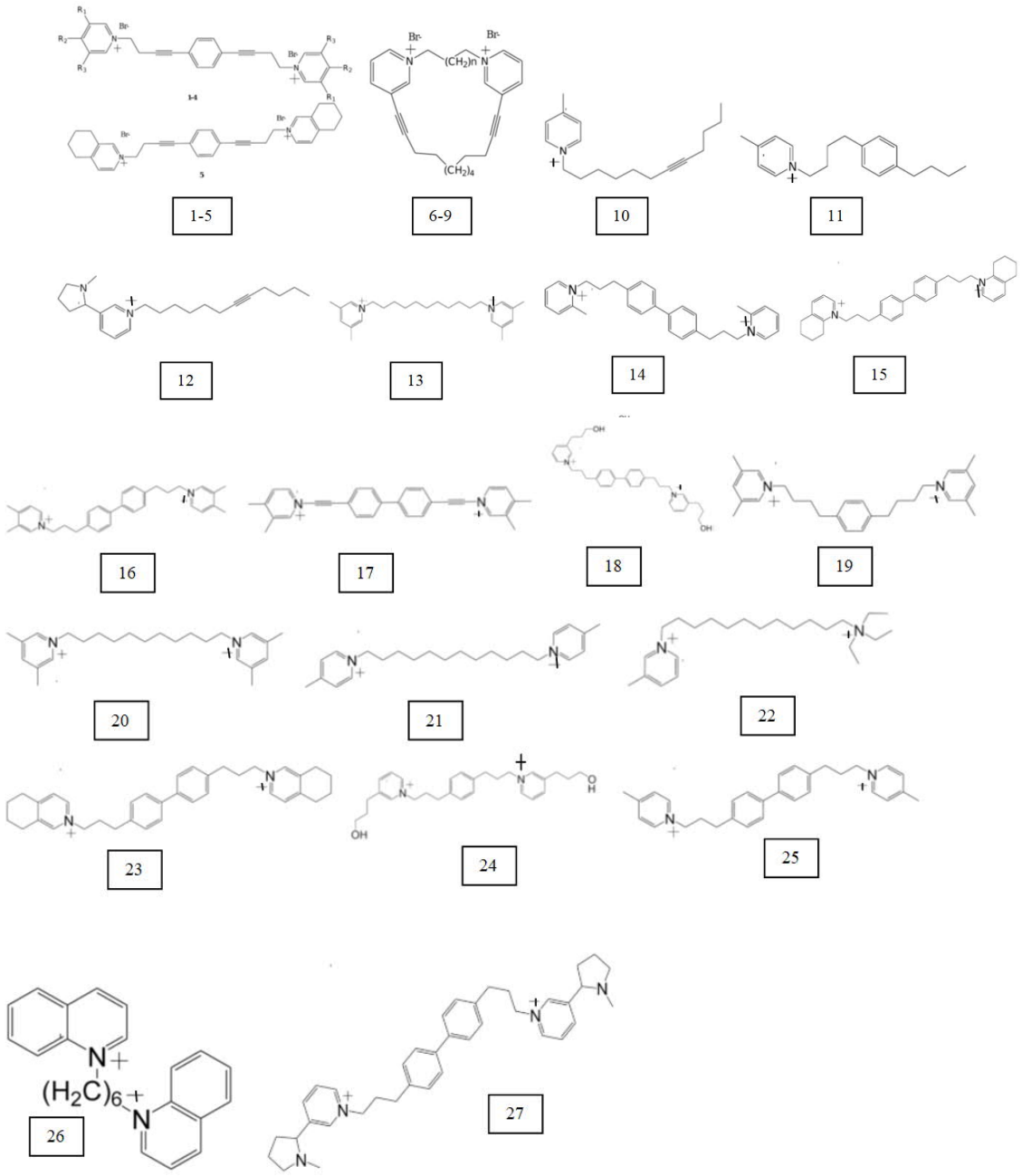

Figure 3. CTL substrate structures [Geldenhuys 2010][9]

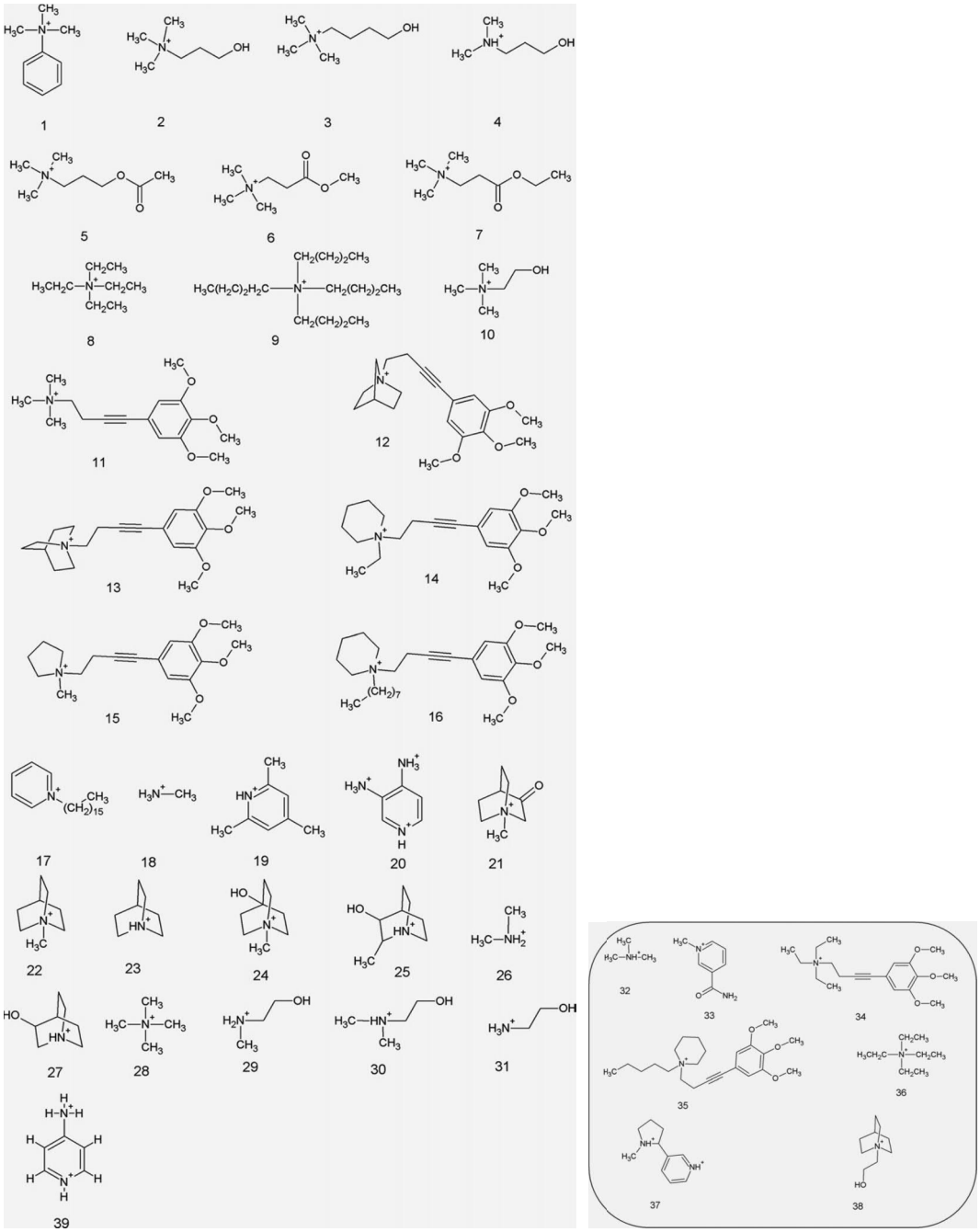

Figure 4. ChT substrate structures [Geldenhuys 2010][33]

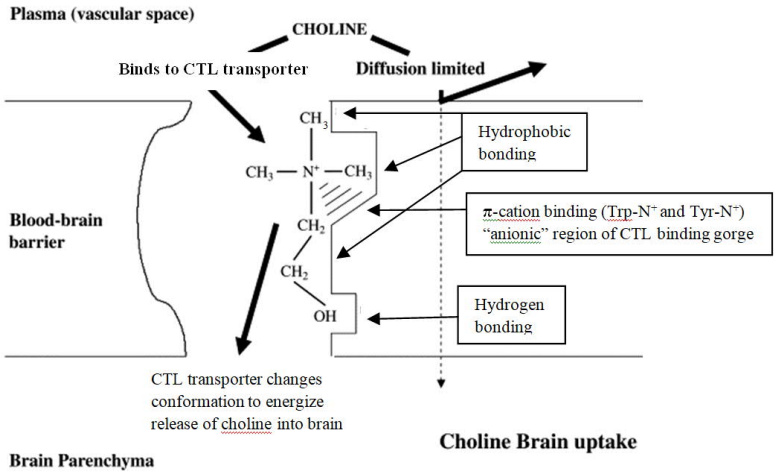

Figure 5(a). Schematic representation of choline transport across blood brain barrier by CTL transporter.

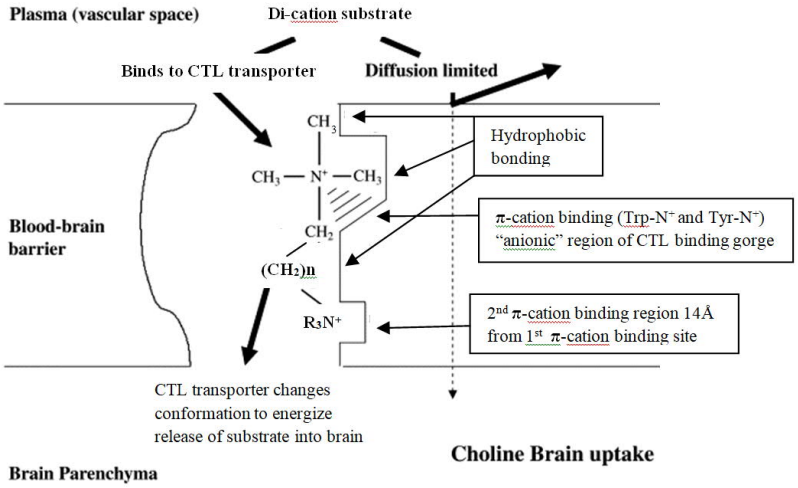

Figure 5(b). Schematic representation of di-cation substrate transport across blood brain barrier by CTL transporter.

AChE Inhibitors	IC_{50} nm	$\Delta G_{desolv,CDS}$ kcal/mol	$\Delta G_{lipo,CDS}$ kcal/mol	DM D	LUMO eV	Vol cm^3/mol	HOMO eV
9	150	-8.04	-10.61	37	-1.54809	263	-6.69143
13E	5.7	-10.45	-9.72	34.73	-1.52741	277	-6.07372
13F	81	-9.09	-10.19	35	-1.58347	28	-6.07834
13G	6.4	-9.08	-10.14	36.53	-1.49802	275	-6.6868
13K	36	-10.4	-9.79	38.63	-1.44278	290	-5.64976
13L	20	-10.21	-9.65	37.28	-1.43326	338	-5.89548
13H	12	9.04	-10.21	38.24	-1.54265	299	-6.1627
13I	85	-9.83	-9.36	38.49	-1.58374	327	-5.98827
13J	25	-10.01	-9.49	40.82	-1.3421	296	-6.39074
13M	13	-11.38	-9.42	35.26	-1.5421	288	-6.21849
13O	30	-10.67	-10.21	27.24	-1.52442	300	-6.06964
13P	1.5	-11	-11.08	38.05	-1.51272	326	-6.06256
15B	94	-11.08	-9.42	67.43	-1.72551	262	-6.17168
16A	10	-10.8	-9.75	34.96	-1.52741	333	-6.07372
16B	2	-10.97	-9.94	34.51	-1.52714	293	-6.07372
16C	40	-12.77	-10.02	22.71	-2.77263	267	-6.06882
16D	60	-12.77	-9.86	22.71	-2.77263	267	-6.06882
16E	4	-13.49	-10.03	33.35	-2.78678	326	-6.07562
16F	100	-13.49	-10.03	33.35	-2.78678	326	-6.07562
16G	8.9	-10.02	-10.48	35.39	-1.52496	342	-6.07345
16H	180	-10.77	-10.48	34.87	-1.53367	312	-6.07726
13Q	35	-11.24	-11.34	28.37	-1.50455	325	-6.04868
17	300	-9.78	-9.46	29.21	-0.5075	254	-5.73547
15A	480	-10.29	-9.74	37.63	-1.68007	248	-6.14284
13N	3300	-10.06	-9.07	29.5	-1.56142	264	-6.07399
13B	5400	-8.64	-6.46	35.38	-1.52904	190	-6.07481

Table 3. Acetylcholinesterase inhibitors (Donepezil analogs) as per structures in Table 1 IC_{50} values from Sugimoto 1995 [31]

AChE Inhibitors	IC_{50} nM	$\Delta G_{desolv,CDS}$ kcal/mol	$\Delta G_{lipo,CDS}$ kcal/mol	DM D	LUMO ev	Vol cm^3/mol	HOMO eV
1a	93600	-12.09	-12.09	19.98	-3.15632	232	-6.96301
1b	8320	-11.86	-11.86	26.37	-3.1321	254	-6.95756
1c	1360	-12.59	-12.59	24.46	-3.13863	266	-6.95294
1d	474	-12.49	-12.49	30.74	-3.11469	282	-6.96382
1e	1780	-13.35	-13.35	36.92	-3.13428	291	-6.94233
1f	8250	-13.61	-13.61	42.67	-3.12203	289	-6.94559
1g	2790	-13.84	-13.84	48.93	-3.13265	346	-6.94369
1h	12300	-12.14	-12.14	19.97	-3.15632	283	-6.95947
1i	252	-11.91	-11.91	26.35	-3.13074	271	-6.95185
1j	151	-12.69	-12.69	24.38	-3.13782	273	-6.93906
1k	607	-12.58	-12.58	30.76	-3.11387	299	-6.95484
1l	4530	-13.32	-13.32	37.01	-3.13428	316	-6.93607
1m	56200	-12.46	-12.46	19.89	-3.15387	319	-6.95212
1n	495	-12.35	-12.35	26.56	-3.13047	346	-6.95267
1o	824	-12.99	-12.99	24.3	-3.13809	328	-6.94396
1p	44000	-12.46	-12.46	19.98	-3.15605	226	-6.95756
1q	1870	-12.18	-12.18	26.32	-3.13047	269	-6.95022
1r	2650	-12.91	-12.91	24.36	-3.13836	328	-6.93988
1s	3370	-9.64	-9.64	18.51	-2.2722	293	-6.94559
1t	637	-12.42	-12.42	20.86	-2.96284	292	-6.94777
1u	1750	-10.09	-10.09	17.86	-2.20472	290	-6.85443
1v	1330	-9.79	-9.79	20.7	-2.41017	283	-6.94668
1w	701	-11.03	-11.03	17.08	-2.15601	303	-6.39618
1x	328	-11.8	-11.8	21.94	-2.30921	307	-6.42285
1y	380	-11.11	-11.11	17.59	-2.45398	321	-6.94668
1z	23.9	-14.12	-14.12	24.95	-3.13809	282	-6.1559
1aa	44.8	-13.85	-13.85	26.02	-3.13809	328	-6.34529
1bb	269	-14.04	-14.04	24.22	-3.13836	358	-6.15182
1cc	0.38	-15.1	-15.1	24.43	-3.12149	299	-6.66395
1dd	18500	-9.27	-9.27	19.31	-0.62207	260	-6.95022
1ee	1090	-9.12	-9.12	18.61	-2.27383	315	-7.08056
1ff	100000	-13.03	-13.03	49.76	-3.14435	313	-3.96098

Table 4. TAK-147 inhibitors of AChE as per structures in Table 2, IC_{50} values from Ishihara 2000 [32]

Substrate	logKi	$\Delta G_{desolv,CDS}$ kcal/mol	$\Delta G_{lipo,CDS}$ kcal/mol	DM D	LUMO eV	Vol cm^3/mol	HOMO ev
1	0.595	-10.61	-13.03	130.27	-2.09941	309	-6.0446
2	0.929	-10.78	-12.91	130.38	-1.94729	263	-6.0427
3	0.924	-11.35	-13.49	130.25	-1.93559	315	-6.02855
4	0.867	-11.58	-13.43	130.39	-2.09043	328	-6.03317
5	0.732	-10.1	-16.53	4.78	-1.92062	344	-6.02963
7	1.529	-10.34	-13.67	17.31	-2.39248	336	-6.88763
9	1.182	-12.07	-16.59	4.54	-2.35166	386	-6.88028
10	2.58	-7.79	-9.52	25.39	-1.89586	255	-6.68055
11	2.69	7.72	-10.15	25.26	-1.89559	207	-6.2144
12	1.92	-9.75	-10.95	48.56	-6.17685	293	-7.82944
13	1.81	-10.2	-12.58	27.97	-1.89586	323	-7.49827
14	2	-9.77	-14.41	11.84	-1.9892	368	-5.89657
15	1.37	-10.17	-17.22	9.58	-1.93749	301	-5.76976
16	1.75	-11.41	-15.02	10.8	-1.8662	349	-5.85548
17	1.98	-13.33	-14.21	1.79	-2.70623	291	-6.07698
18	1.86	-13.97	-16.09	4.02	-2.86216	427	-6.16406
20	2.54	-10.53	-13.09	0.35	-1.97396	286	-7.54371
21	1.93	-9.48	-11.95	27.94	-1.82729	255	-7.83379
22	1.34	-10	-11.48	3.73	-2.01777	414	-7.67378
23	1.2	-10.42	-18.05	6.71	-1.85613	443	-5.88786
24	2.09	-10.48	-14.17	1.87	-2.02022	293	-6.3355
25	1.63	-10.75	-14.55	12.36	-1.93232	347	-5.80269
26	1.26	-7.57	-12.29	3.4	-2.52527	261	-6.78694
27	1.73	-7.97	-17.78	11.63	-1.9013	497	-5.76758

Table 5. Transport of 24 cationic substrates across BBB by CTL Transporters, see Figure 3 for CTL substrate structures, Ki values from Geldenhuys 2010 [9]

Substrate	pKi	$\Delta G_{desolv,CDS}$ kcal/mol	$\Delta G_{lipo,CDS}$ kcal/mol	DM D	LUMO eV	Vol cm^3/mol	HOMO eV
1	4.124	-5.55	-4.08	6.02	-0.55322	115	-7.17825
2	5.657	-5.25	-3	6.44	1.618026	89	-7.35921
3	3.508	-5.53	-3.53	9.15	1.628638	116	-7.27458
4	3.537	-5.04	-2.55	7.05	1.554894	93	-7.36738
5	3.721	-7.34	-3.66	17.07	0.149394	152	-7.62752
6	3.5686	-7.38	-2.7	10.43	0.019048	109	-7.82263
7	3.4585	-7.32	-3.71	11.63	0.008436	134	-7.77256
8	4.619	-4.9	-3.31	0.06	1.795176	129	-9.32991
9	2.978	-7.29	-7.23	1.09	1.746466	204	-8.56226
10	6.167	-4.96	-2.47	4.45	1.37339	83	-7.55133
11	5.6989	-18.83	-5.16	26.94	-0.82997	210	-5.90364
12	7.301	-9.67	-7.11	28.27	-0.8218	248	-5.89738
13	7.0457	-9.66	-7.38	27.98	-0.82724	219	-5.89929
14	6.744	-10.2	-7.16	27.54	-0.84085	243	-5.90446
15	6.698	-10.13	-6.51	27.66	-0.75813	190	-5.83561
16	6.638	-11.98	-10.32	13.53	-0.74398	381	-5.78445
17	4.494	-7.75	-11.4	40.11	-2.03002	249	-7.67106
18	1.455	-3.2	0.13	2.76	1.327401	36	-11.161
19	3.97	-4.2	-3.68	2.81	-1.8379	104	-7.50316
20	3.086	-6.07	-1.31	8.3	-3.2668	86	-9.20745
21	6.283	-4.61	-4.43	7.95	-0.98589	93	-7.2373
22	5.3279	-3.63	-4.19	3.37	1.363865	101	-8.52688
23	4.397	-3.3	-3.82	4.41	1.268896	83	-8.5443
24	4.142	-3.98	-4.04	6.43	1.30155	111	-7.44439
25	3.677	-3.9	-3.84	5.47	1.366042	100	-7.61337
26	2.026	-3.98	-0.64	2	1.38237	50	-10.8538
27	3.677	-3.63	-3.72	6.46	1.358151	89	-7.62834
28	4.522	-4.87	-1.85	0.01	1.481421	61	-10.7017
29	2.42	-4.19	-1.52	6.37	1.27842	59	-7.57691
30	4.254	-4.76	-2.04	5.15	1.344817	100	-7.57364
31	0.8239	-3.32	-0.8	8.25	1.19379	56	-7.58752
32	3.4685	-4.66	-1.34	1.22	1.423732	66	-10.7515
33	3.443	-5.41	-2.97	9.88	-2.29669	95.2	-7.58208
34	6.154	-10.93	-6.06	27.37	-0.82425	228	-5.89521
35	7.698	-11.15	-8.63	26.66	-0.81772	282	-5.85766
36	3.585	-4.91	-3.32	0	1.815585	142	-9.35004
37	3.2839	-5.67	-4.58	5.22	-2.38295	112	-8.28007
38	6.1938	-3.95	-4.69	2.24	1.395703	112	-7.51786
39	3.318	-4.82	-1.95	4.86	-2.70188	84	-8.66457

Table 6. Transport of 24 cationic substrates into neurones by ChT Transporters, see Figure 4 for ChT substrate structures, pKi values from Geldenhuys 2010 [33]